Clays and Clay Minerals (2026), **74**, e8, 1–6
doi:10.1017/cmn.2026.10031

Original Paper

Hydration structure and energetics of iron-exchanged montmorillonite

Tuan A. Ho[1] and Carlos F. Jove-Colon[2]

[1]Geomechanics and Geochemistry Department, Sandia National Laboratories, Albuquerque, New Mexico, NM 87185, USA and [2]Nuclear Waste Disposal Research and Analysis Department, Sandia National Laboratories, Albuquerque, New Mexico, NM 87185, USA

Abstract

The interaction between iron released from corroded steel canisters and bentonite is a key process influencing the long-term performance of nuclear waste repositories. In particular, the migration of Fe^{2+} into montmorillonite (Mnt) interlayers may alter its hydration, swelling, and ion-transport properties. In the present study, molecular dynamics simulations were performed to investigate the hydration behavior, structural response, and transport properties of Fe-exchanged montmorillonite (Fe-Mnt) under varying hydration states. The simulations focus on short- to intermediate-time-scale Fe^{2+} and Fe^{3+} interlayer exchange and hydration effects, and do not consider long-term structural substitution, Fe-bearing clay phase stabilization, or secondary iron mineral precipitation. Systems containing Na^{+}-, Fe^{2+}-, and Fe^{3+}-Mnt were examined using both periodic and edge-exposed configurations to evaluate interlayer structure, ion exchange, and free energy of Fe intercalation. The results show that Fe ions influence the interlayer spacing primarily at low water contents (<1 bilayer), where Fe-Mnt exhibits a *d*-spacing 1–2 Å larger than Na-Mnt due to stronger hydration. The calculated hydration energies follow the order Fe^{2+}<Fe^{3+}<Na^{+}. Both water and ion diffusion coefficients decrease upon Fe ion intercalation, with Fe^{2+} ions diffusing an order of magnitude more slowly than those of Na^{+}. Free energy profiles further confirm that Fe^{2+} and Fe^{3+} ions are thermodynamically favored in the interlayer, with Fe^{3+} being the most stable. These findings provide molecular-scale insights into the mechanisms of Fe–Na exchange and their implications for bentonite alteration in repository environments.

Keywords: clay; clay swelling; corrosion; ion exchange; nuclear waste repository

(Received: 17 November 2025; revised: 16 March 2026; accepted: 19 March 2026)

Introduction

In many nuclear waste repository concepts, metallic canisters (e.g. steel) are buried in deep tunnels with bentonite used as backfill material. Upon repository closure, elevated temperatures and variable water-saturation conditions promote canister corrosion, releasing iron species into the bentonite. Numerous studies (Kaufhold et al., 2015; Latta et al., 2017), including the FEBEX *in situ* heater test at the Grimsel Test Site in Switzerland (Hadi et al., 2019) have documented the resulting alteration of bentonite in close proximity to steel material. Diffusion of iron species into the bentonite has resulted in the formation of large (>140 mm wide) red, orange, and blue regions due to the formation of iron minerals such as goethite. Excess Fe^{2+} ions may also diffuse far away from the container interface and adsorb onto the clay surface.

In contrast to the formation of goethite in the work by Kaufhold et al. (2015), Milodowski et al. (2007) concluded that the bentonite immediately adjacent to the steel canister was significantly enriched in iron, not as iron oxide or iron oxyhydroxide but through the substitution of iron into the octahedral layers of bentonite, forming minerals such as nontronite. The cation exchange capacity (CEC) of altered bentonite is slightly reduced, with depletions in exchangeable Ca^{2+} and Na^{+} and an increase in exchangeable Fe^{2+}. In general, bentonite interaction with iron has been shown to reduce shrinkage significantly, possibly due to its conversion to nontronite and chlorite (Jones et al., 2017).

Laboratory studies further showed that sorbed Fe^{2+} on clays can undergo redox transformations. Under anoxic conditions, Fe^{2+} sorbed onto low-iron clay surfaces can be partly oxidized to Fe^{3+}, forming Fe(III)-bearing minerals (Géhin et al., 2007; Van Groeningen et al., 2020). When exposed to air, this oxidation proceeds rapidly and completely, demonstrating that clay minerals were unable to protect ferrous iron from oxidation. Nonetheless, Fe^{2+} can persist in clay interlayers under reducing conditions as the conversion to Fe(III) in anoxic conditions is only partial. Furthermore, Manjanna (2008) prepared Fe^{2+}-Mnt successfully by reducing Fe^{3+}-Mnt and suggested that, for long-time preservation, Fe^{2+}-montmorillonite must be stored in deoxygenated and/or low relative humidity (<40%) conditions at room temperature or below. A further report suggested that iron adsorption at 2<pH<7.5 occurs both via cation exchange on interlayer surfaces and as sorption onto highly reactive surface sites (e.g. edge and defect) (Géhin et al., 2007). The conversion from Fe^{2+} to Fe^{3+} increases with pH. This reaction is reversible (e.g. reducing the pH can reduce Fe^{3+} to Fe^{2+} in solution).

Corresponding author: Tuan A. Ho; Email: taho@sandia.gov

Cite this article: Ho T.A., & Jove-Colon C.F. (2026). Hydration structure and energetics of iron-exchanged montmorillonite. *Clays and Clay Minerals* **74**, e8, 1–6. https://doi.org/10.1017/cmn.2026.10031

© The Author(s), 2026. Published by Cambridge University Press on behalf of The Clay Minerals Society.

https://doi.org/10.1017/cmn.2026.10031 Published online by Cambridge University Press

The adsorption of Fe^{2+} onto clay depends significantly on structural Fe. On a low-Fe content clay or dithionite-reduced clays, Fe^{2+} uptake generally follows the sorption behavior of other divalent metals (Soltermann et al., 2014a), primarily through cation exchange and surface complexation with clay edges or surface defects, which are highly pH dependent. When Fe^{2+} adsorbs onto Fe(III)-rich clays, the amount of Fe adsorbed is unexpectedly large (Schaefer et al., 2011; Soltermann et al., 2014a), possibly due to electron transfer between sorbed Fe^{2+} and structural Fe(III). In low-Fe clays, sorbed Fe^{2+} can be partially oxidized to mineral-bound Fe(III) complexes, whereas in high Fe-clays, sorbed Fe^{2+} is fully oxidized.

Despite this progress, the reaction pathways remain unclear. Aqueous Fe^{2+} may: (1) adsorb to basal surfaces by cation exchange; (2) form adsorption complexes at edge sites; (3) precipitate as secondary minerals; or (4) undergo interfacial redox reactions with structural Fe(III) (O'Reilly et al., 2005; Merola et al., 2007; Jaisi et al., 2008; Schaefer et al., 2011; Soltermann et al., 2014a; Soltermann et al., 2014b; Van Groeningen et al., 2020). The latter pathway suggests Fe^{2+} intercalation into clay interlayers with electron transfer to structural Fe(III), a process influenced by Fe^{2+} concentration and Fe(III) accessibility. Such redox-driven intercalation could alter surface charge, CEC, and swelling/shrinkage behavior, while simultaneously promoting secondary mineral formation such as that of chlorite. This background points to a key knowledge gap: the behavior and hydration of Fe^{2+} in clay interlayers under repository-relevant conditions. Accordingly, while Fe-montmorillonite interactions may involve surface sorption, structural substitution, redox transformations, and secondary mineral precipitation, the present study focused specifically on Fe^{2+} interlayer exchange and hydration, and does not address long-term structural incorporation, Fe-bearing clay phase stabilization, or secondary mineral formation. The hypothesis is that Fe^{2+} generated from canister corrosion can exchange with interlayer Na^+ in montmorillonite, modifying its hydration and structural properties. Evidence has been found for Fe^{2+}/Na^+ exchange in smectite interlayers under reducing conditions (Kamei et al., 1999), reinforcing this possibility. In the present study, molecular dynamics simulation was used to investigate the hydration structural properties and energetics of iron ion intercalation into the clay interlayer space.

Materials and methods

To address the knowledge gap about the hydration and structure of iron-exchanged Mnt, molecular dynamics simulations were used to investigate Fe-Mnt hydration properties. The simulation system including two clay layers with the *x*–*y* surface area of 4.1 nm×3.5 nm is presented in Fig. 1a. The clay structure was prepared by replicating a unit cell by 8×4×2 in *x*, *y*, and *z*-dimensions. The montmorillonite structure adopts a dioctahedral *cis*-vacant configuration, which is prevalent in engineered clay barrier materials (Drits and Zviagina, 2009; Subramanian et al., 2020). A previous study (Gao et al., 2025) has shown that *cis*- and *trans*-vacant montmorillonite exhibit similar interlayer hydration behaviors; nevertheless, the vacancy configuration is provided here for completeness. For all systems, isomorphic substitution occurred in octahedral sheets. Different numbers of water molecules were placed in the interlayer spaces to create hydrated structures, and the amount of water in the interlayers was expressed as the number of water molecules per unit cell of clay, i.e. w u.c.$^{-1}$. Interlayer ions, Na^+, Fe^{2+}, or Fe^{3+}, were placed in the interlayer space also to balance the structural charge. There were 24 Na^+ ions in each interlayer, and when Fe^{2+} or Fe^{3+} replaced Na^+, their number was adjusted according to the charge.

In the simulations in Fig. 1a, Na^+ ions were replaced by Fe ions in the interlayer spaces without studying the exchange reaction explicitly. The simulation in Fig. 1b focused on ion exchange in clay because it is one of the fundamental processes in the bentonite buffer, e.g. radionuclide exchange for Na^+ in bentonite; Ca^{2+}, Mg^{2+} exchange for Na^+ ions in the interlayers leading to a change in the concentration of the ions (Kaufhold et al., 2018). The system in Fig. 1b is different from that in Fig. 1a as the clay particles have edges along the *x*-direction which expose the interlayers to aqueous solutions while the system in Fig. 1a is periodic (e.g. infinitely long) in the *x*-direction. The system in Fig. 1b allows the exchange of water and ions in the interlayer spaces with those in bulk aqueous solution. The method for constructing clay particles with edges can be found in previous studies by the present authors (Ho et al., 2019; Ho et al., 2020; Ho et al., 2022; Ho et al., 2023b). Exchange reactions via equilibrium simulations and free-energy calculation were studied here. In the equilibrium simulations, iron chloride was added to the bulk regions and the amount of iron ions moving into the interlayer was monitored. In the free-energy calculation, a metadynamics technique (Barducci et al., 2008) was applied using the Colvars module (Fiorin et al., 2013) to calculate the free energy of Fe^{2+} or Fe^{3+} ions moving from bulk water into the interlayer space. Such free-energy landscapes provide a comprehensive evaluation about energy barrier and thermodynamics of iron intercalations. This technique has been applied to calculate gas intercalation into the clay interlayer space (Ho et al., 2023b; Choudhary and Ho, 2024); this includes hydrogen generated from canister corrosion being intercalated into bentonite which is relevant to the nuclear repository (Ho et al., 2023a). A summary of simulated systems is reported in Table 1.

The *ClayFF* force field (Cygan et al., 2004) was used to simulate clay with additional Si-O-H and Al-O-H angle terms describing edge hydroxyl groups (Pouvreau et al., 2017; Pouvreau et al., 2019).

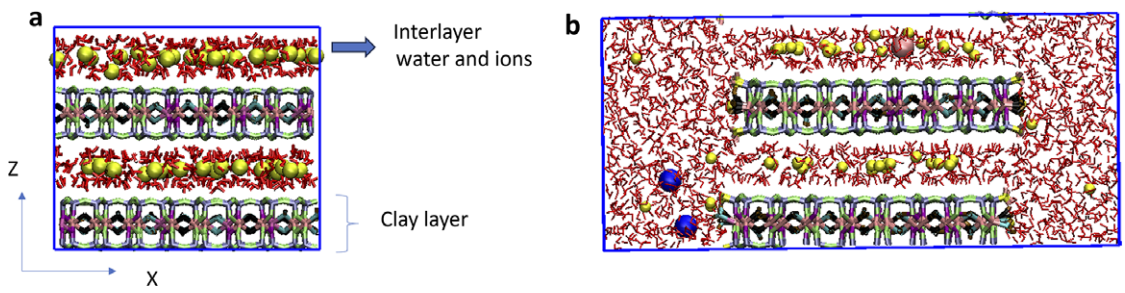


Figure 1. (a) Simulation snapshot demonstrating the periodic clay system including two clay layers and two interlayers with water and ions to study hydration properties of Na^+, Fe^{2+}, and Fe^{3+}. (b) Clay system with edge to study the exchange reaction of Fe^{2+} (pink) with Na^+ (yellow). Cl^- (blue) balances the charge of Fe^{2+}.

https://doi.org/10.1017/cmn.2026.10031 Published online by Cambridge University Press

Table 1. Systems simulated and the corresponding number of ions

System	Number of ions in the system	Results
Periodic structure (Fig. 1a)	48 Na^+	Fig. 2a, Fig. 3, Fig. 4
Periodic structure (Fig. 1a)	24 Fe^{2+}	Fig. 2a, Fig. 3, Fig. 4
Periodic structure (Fig. 1a)	16 Fe^{3+}	Fig. 2a, Fig. 3
Periodic structure (Fig. 1a)	24 Na^+ and 12 Fe^{2+}	Fig. 2b
Edge structure (Fig. 1b)	1 Fe^{2+}, 2 Cl^- and 48 Na^+	Fig. 5
Edge structure (Fig. 1b)	1 Fe^{3+}, 3 Cl^- and 48 Na^+	Fig. 5

Water molecules were simulated using a flexible SPC water model (Teleman et al., 1987), and the Na^+ ion was modeled using the force field proposed by Smith and Dang (1994). Iron-water force-field parameters were taken from Babu and Lim (2006). Fe^{2+} and Fe^{3+} have the same Lennard-Jones parameters and have charges of +2 and +3, respectively. Fe^{2+} and Fe^{3+} were modeled using non-reactive force fields that treat Fe as fully solvated cations interacting electrostatically with water molecules and clay surfaces. These force fields were selected because they have been applied widely in classical molecular dynamics studies of hydrated metal cations and ion-clay systems, and they provide a computationally efficient framework for comparing interlayer hydration and swelling behavior systematically across various exchangeable cations. The present model does not account for hydrolysis reactions or for the formation of Fe-hydroxyl coordination complexes in aqueous solution. Instead, the simulations were designed to represent Fe cations under conditions where aqueous speciation and redox reactions are suppressed, allowing the effects of ionic charge and hydration strength on interlayer structure to be isolated. The Lennard-Jones (LJ) potential was expressed as: $V_{LJ} = 4\varepsilon\left[\left(\frac{\sigma}{r}\right)^{12} - \left(\frac{\sigma}{r}\right)^{6}\right]$, where r is the distance between two atoms, and ε and σ are the depth of the potential energy well and the distance at which the LJ potential is zero, respectively. LJ interactions among atoms were calculated using the Lorentz-Berthelot mixing rules: $\varepsilon_{ij} = \sqrt{\varepsilon_{ii}\varepsilon_{jj}}$ and $\sigma_{ij} = \left(\sigma_{ii} + \sigma_{jj}\right)/2$. Short-range interactions were calculated using a cut-off distance of 10 Å. Long-range electrostatic interactions were calculated using the PPPM (particle-particle-particle-mesh) solver (Hockney and Eastwood, 1988). All simulations were performed using the *LAMMPS* package (Plimpton, 1995) at a temperature of 300K, pressure of 1 atm using the Nose-Hoover thermostat (Nose, 1984) and barostat, and a timestep of 1 fs.

Results and Discussion

The *d*-spacing of Mnt systems containing 100% Na^+, Fe^{2+}, or Fe^{3+} ions in the interlayers is shown in Fig. 2a. These results were obtained from the simulation system shown in Fig. 1a. The results indicate that Fe ions influence the *d*-spacing primarily at low water contents (e.g. <7 water molecules per unit cell, or w u.c.$^{-1}$). In other words, when Na^+ ions were completely replaced by either Fe^{2+} or Fe^{3+}, changes in the *d*-spacing of Mnt were observed only when the interlayer contains less than a bilayer of water (*d*-spacing <14 Å). At higher water contents, beyond the bilayer region

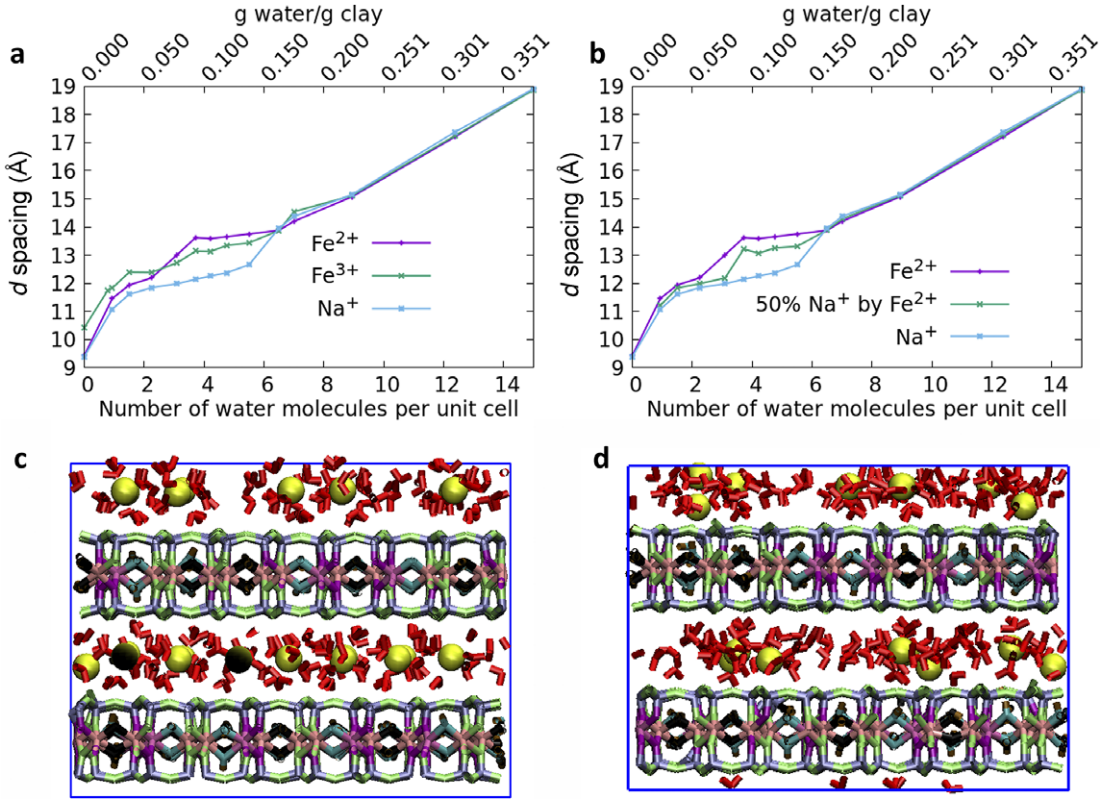


Figure 2. (a) d-spacing as a function of the number of water molecules per clay unit cells (or water mass per clay mass without considering mass of ions) for Fe^{2+}, Fe^{3+}, and Na^+ montmorillonite. (b) Comparison of d-spacing in montmorillonite when 50% of the Na^+ ions in the interlayer space are replaced by Fe^{2+} ions, along with those of pure Na^+- and Fe^{2+}-montmorillonite. (c, d) Simulation snapshots for Fe^{2+} and Fe^{3+} systems at 3.71 w u.c.$^{-1}$, respectively.

https://doi.org/10.1017/cmn.2026.10031 Published online by Cambridge University Press

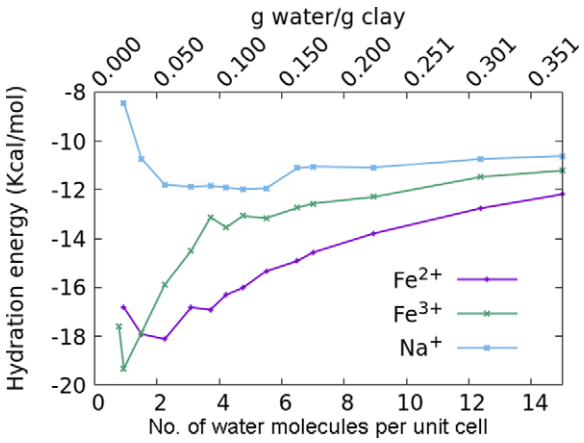


Figure 3. Comparison of hydration energies for Na^+-, Fe^{2+}-, and Fe^{3+}-montmorillonite.

(*d*-spacing >14 Å), the type of interlayer cation (Na^+, Fe^{2+}, or Fe^{3+}) has little effect on the swelling behavior of the clay. When the water content is less than a bilayer, the *d*-spacing of Fe-Mnt is ~1–2 Å larger than that of Na-Mnt at equivalent hydration levels. This difference arises from the greater hydration energy of Fe ions compared with Na^+, which leads to a larger hydration shell surrounding the Fe ions. Simulation snapshots in Fig. 2c, d show that at a water content of 3.7 w u.c.$^{-1}$, water molecules are more evenly distributed in the Fe^{2+} system than in the Fe^{3+} system. Because there are fewer interlayer ions in the Fe^{3+} case and Fe^{3+} attracts water more strongly due to its higher charge, water molecules are more tightly coordinated around the ions. This leads to a smaller *d*-spacing in Fe^{3+} compared with Fe^{2+}.

The expansion of the clay varies with increasing amount of Fe^{2+} in the interlayer space compared with Na^+ ions. For example, the *d*-spacing of Fe^{2+}-Mnt and Na-Mnt is compared with that of Mnt containing both Fe^{2+} and Na^+ in the interlayer (i.e. Fe–Na-Mnt) in Fig. 2b. At low water contents, the *d*-spacing increases in the order Na-Mnt<Fe–Na-Mnt<Fe-Mnt. Therefore, depending on the extent of Fe ion exchange for Na^+ in the interlayer space, the clay can exhibit different swelling behaviors. The present *d*-spacing results for Fe-Mnt and Na-Mnt are consistent with the experimental findings of Manjanna (2008).

The hydration energies for Na^+-, Fe^{2+}-, and Fe^{3+}-montmorillonite obtained from the simulation system (Fig. 1a) are shown in Fig. 3. The hydration energy was defined as the change in potential energy, *U*, associated with adding *n* water molecules to a dry (*n*=0) clay system:

$$\Delta U(n) = \frac{U(n) - U(n=0)}{n}.$$

The results for Na^+ agree well with those of Teich-McGoldrick et al. (2015). As the number of water molecules increased, the hydration energy approached the value characteristic of bulk water (~10 kcal mol^{-1}). The hydration energy exhibited a minimum at low water content (<1 monolayer of water). The profile for Fe^{2+} is similar to that of other divalent cations (Teich-McGoldrick et al., 2015), showing a sharper minimum compared with the broader minimum observed for monovalent ions. The hydration energy of Fe^{3+} is generally lower (i.e. more negative) than that of Na^+ but greater than that of Fe^{2+}. Note that the hydration energy differs from hydration free energy, which includes entropic contributions. Such entropic effects have been examined in previous studies (Whitley and Smith, 2004; Zhou et al., 2020; Li et al., 2023).

The diffusion coefficients of water and ions are reported in Fig. 4 for the interlayer space of the system shown in Fig. 1a, to examine how the exchange of Fe ions for Na^+ ions affects the transport properties of the ions and water. The results indicate that both water (Fig. 4a) and ions (Fig. 4b) diffuse more slowly in Fe-Mnt than in Na-Mnt. While the difference in water diffusion between Na-Mnt and Fe-Mnt is not substantial, Fe^{2+} ions diffuse much more slowly, by at least an order of magnitude, compared with Na^+ ions. The results in Fig. 4 also suggest that the diffusion of both water and ions depends heavily on the amount of water present in the interlayers.

As mentioned above, in the simulations shown in Fig. 1a, the Na^+ ions were replaced with Fe ions in the interlayer spaces without explicitly modeling the exchange reaction. To investigate the intercalation of iron ions from the bulk solution into the interlayer space initially occupied by Na^+ ions, the system shown in Fig. 1b was used. For example, the positions of five Fe^{3+} ions that were initially placed in the bulk solution are shown in Fig. 5a. The presence of Fe^{3+} ions in the interlayer indicates that, within a few nanoseconds of the simulation, Fe^{3+} ions had already migrated into the interlayer. The free energy of ion exchange between the bulk and the interlayer is reported in Fig. 5b. The data indicate that both Fe^{2+} and Fe^{3+} are thermodynamically more stable within the interlayer space than in the bulk solution, with Fe^{3+} being more favorable. In the edge-exposed

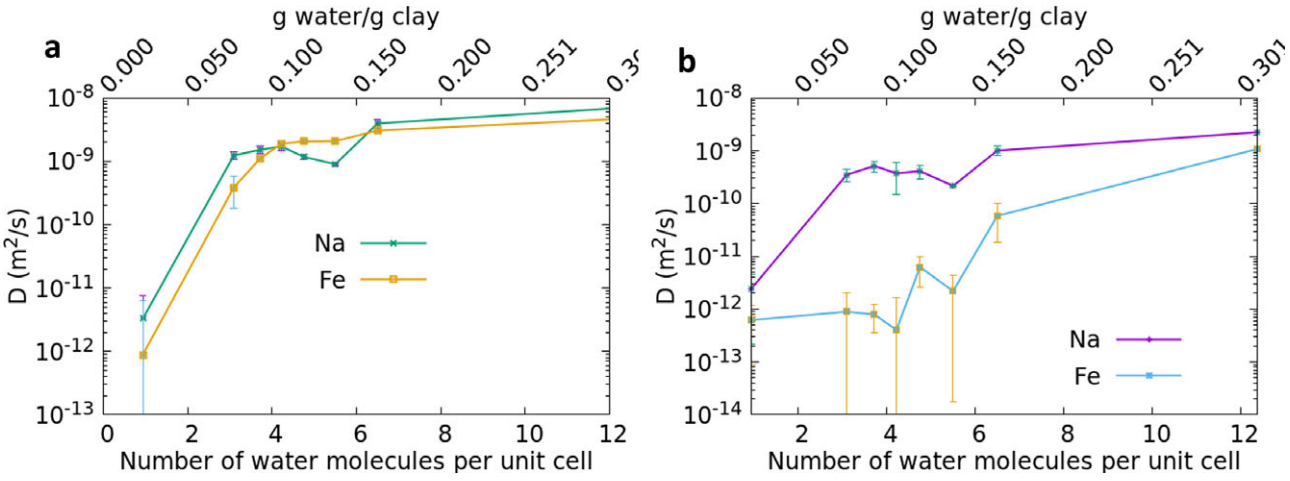


Figure 4. (a) Comparison of water diffusion coefficients in Na^+- and Fe^{2+}-Mnt. (b) Diffusion coefficients of Na^+ and Fe^{2+} ions in the interlayers.

https://doi.org/10.1017/cmn.2026.10031 Published online by Cambridge University Press

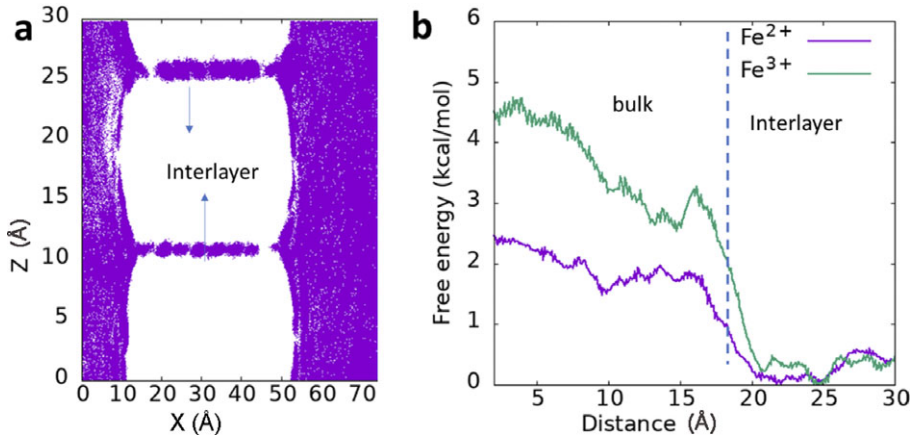


Figure 5. (a) Positions of five Fe^{3+} ions throughout the simulation of the system shown in Fig. 1b. (b) Potential of mean force for the exchange of an iron ion between the bulk solution and the interlayer space.

simulation set-up used to calculate the potential of mean force (PMF), both ions and water molecules were free to exchange dynamically between the interlayer and the bulk solution. As Fe^{2+} or Fe^{3+} migrates from the bulk across the clay edge into the interlayer space, this process is inherently coupled to water redistribution, including partial dehydration in the bulk clay, reorganization of hydration shells, and rehydration under interlayer confinement. These solvent rearrangements were captured explicitly in the PMF and contribute to both energetic and entropic components of the free-energy landscape. Consequently, the calculated PMF profiles reflect not only ion–clay electrostatic interactions, but also the cost of water displacement and confinement effects during ion intercalation, explaining the distinct barriers and stability observed for Fe^{2+} and Fe^{3+}.

Conclusions

The simulations shown here demonstrated that the exchange of Na^+ by Fe^{2+} or Fe^{3+} in montmorillonite interlayers influences the clay's structural and transport properties significantly, particularly at low water content. Fe ions increase the *d*-spacing by 1–2 Å compared with Na-Mnt when the interlayer contains less than a bilayer of water, reflecting their stronger hydration. Hydration-energy calculations reveal that Fe^{2+} and Fe^{3+} form more stable hydration shells than Na^+, with the order Fe^{2+}<Fe^{3+}<Na^+. The diffusion of both water and ions decreases in Fe-Mnt, with Fe^{2+} ions exhibiting much slower mobility than Na^+, suggesting that Fe enrichment can impede interlayer transport. Free-energy profiles indicate that both Fe^{2+} and Fe^{3+} intercalate preferentially into the clay interlayers, highlighting the thermodynamic favorability of Fe–Na exchange under repository-relevant conditions. These findings imply that Fe-enriched smectites can form near corroded canisters, altering bentonite swelling (e.g. at the same water content as in the interlayer, Fe-exchanged Mnt swells more than Na-exchanged Mnt), CEC, and potentially its long-term performance as a buffer material in nuclear waste repositories.

Author contributions. TAH and CFJ designed the research and wrote the paper. TAH conducted simulations and analyzed data.

Acknowledgments. The authors thank Dr Jeffery Greathouse of Sandia National Laboratories for valuable discussions.

Data availability statement. The authors confirm that the data supporting the findings of this study are available within the article or can be made available through appropriate requests.

Financial support. This work was supported by the DOE Spent Fuel and Waste Science & Technology (SFWST) Program. This article was co-written by an employee of National Technology & Engineering Solutions of Sandia, LLC under Contract No. DE-NA0003525 with the U.S. Department of Energy (DOE). The employee owns all right, title and interest in and to the article and is solely responsible for its contents. The United States Government retains, and the publisher, by accepting the article for publication, acknowledges that the United States Government retains a non-exclusive, paid-up, irrevocable, world-wide licence to publish or reproduce the published form of this article or allow others to do so, for United States Government purposes. The DOE will provide public access to these results of federally sponsored research in accordance with the DOE Public Access Plan: https://www.energy.gov/downloads/doe-public-access-plan.

Competing interests. The authors declare that they have no competing interests.

References

Babu, C.S., & Lim, C. (2006). Empirical force fields for biologically active divalent metal cations in water. *Journal of Physical Chemistry A*, *110*, 691–699.

Barducci, A., Bussi, G., & Parrinello, M. (2008). Well-tempered metadynamics: a smoothly converging and tunable free-energy method. *Physical Review Letters*, *100*, 020603.

Choudhary, A., & Ho, T.A. (2024). Confinement-induced clustering of H_2 and CO_2 gas molecules in hydrated nanopores. *Physical Chemistry Chemical Physics*, *26*, 10506–10514.

Cygan, R.T., Liang, J.J., & Kalinichev, A.G. (2004). Molecular models of hydroxide, oxyhydroxide, and clay phases and the development of a general force field. *Journal of Physical Chemistry B*, *108*, 1255–1266.

Drits, V.A., & Zviagina, B.B. (2009) Trans-vacant and cis-vacant 2:1 layer silicates: structural features, identification, and occurrence. *Clays and Clay Minerals*, *57*, 405–415.

Fiorin, G., Klein, M.L., & Hénin, J. (2013). Using collective variables to drive molecular dynamics simulations. *Molecular Physics*, *111*, 3345–3362.

Gao, P., Zhang, Y., Liu, X., & Lu, X. (2025). A molecular dynamics study of swelling, structural and dynamic properties of 2:1 cis-vacant Cs saturated smectite. *Applied Clay Science*, *270*, 107788.

Géhin, A., Grenèche, J.-M., Tournassat, C., Brendlé, J., Rancourt, D.G., & Charlet, L. (2007). Reversible surface-sorption-induced electron-transfer oxidation of Fe(II) at reactive sites on a synthetic clay mineral. *Geochimica et Cosmochimica Acta*, *71*, 863–876.

Hadi, J., Wersin, P., Serneels, V., & Grenèche, J.-M. (2019). Eighteen years of steel–bentonite interaction in the FEBEX in situ test at the Grimsel Test Site in Switzerland. *Clays and Clay Minerals*, *67*, 111–131.

https://doi.org/10.1017/cmn.2026.10031 Published online by Cambridge University Press

Ho, T.A., Criscenti, L.J., & Greathouse, J.A. (2019). Revealing transition states during the hydration of clay minerals. *Journal of Physical Chemistry Letters*, *10*, 3704–3709.

Ho, T.A., Wang, Y., Jové Colón, C.F., & Coker, E.N. (2020). Fast advective water flow through nanochannels in clay interlayers: implications for moisture transport in soils and unconventional oil/gas production. *ACS Applied Nano Materials*, *3*, 11897–11905.

Ho, T.A., Coker, E.N., Jové-Colón, C.F., & Wang, Y. (2022). Control of structural hydrophobicity and cation solvation on interlayer water transport during clay dehydration. *Nano Letters*, *22*, 2740–2747.

Ho, T.A., Jove-Colon, C.F., & Wang, Y. (2023a). Low hydrogen solubility in clay interlayers limits gas loss in hydrogen geological storage. *Sustainable Energy & Fuels*, *7*, 3232–3238.

Ho, T.A., Yang, W., Rempe, S.B., Dasgupta, N., Johnston, C.T., Xu, G., Zwier, T. S., & Mills, M. (2023b). Control of the structural charge distribution and hydration state upon intercalation of CO_2 into expansive clay interlayers. *Journal of Physical Chemistry Letters*, *14*, 2901–2909.

Hockney, R.W., & Eastwood, J.W. (1988). *Computer Simulation Using Particles*, 564 pp. Taylor & Francis Group, LLC, New York.

Jaisi, D.P., Liu, C., Dong, H., Blake, R.E., & Fein, J.B. (2008). Fe^{2+} sorption onto nontronite (NAu-2). *Geochimica et Cosmochimica Acta*, *72*, 5361–5371.

Jones, A.M., Murphy, C.A., Waite, T.D., & Collins, R.N. (2017). Fe(II) interactions with smectites: temporal changes in redox reactivity and the formation of green rust. *Environmental Science & Technology*, *51*, 12573–12582.

Kamei, G., Oda, C., Mitsui, S., Shibata, M., & Shinozaki, T. (1999). Fe(II)–Na ion exchange at interlayers of smectite: adsorption–desorption experiments and a natural analogue. *Engineering Geology*, *54*, 15–20.

Kaufhold, S., Hassel, A.W., Sanders, D., & Dohrmann, R. (2015). Corrosion of high-level radioactive waste iron-canisters in contact with bentonite. *Journal of Hazardous Materials*, *285*, 464–473.

Kaufhold, S., Dohrmann, R., Ufer, K., & Kober, F. (2018). Interactions of bentonite with metal and concrete from the FEBEX experiment: mineralogical and geochemical investigations of selected sampling sites. *Clay Minerals*, *53*, 745–763.

Latta, D.E., Neumann, A., Premaratne, W.A.P.J., & Scherer, M.M. (2017). Fe (II)–Fe(III) electron transfer in a clay mineral with low Fe content. *ACS Earth and Space Chemistry*, *1*, 197–208.

Li, Q., Lu, X., Chen, M., Zhang, L., Cheng, Y., Liu, X., & Yin, Z. (2023). Lithium partition and isotopic fractionation for cation exchange in clay: insights from molecular simulations. *Geochimica et Cosmochimica Acta*, *358*, 148–161.

Manjanna, J. (2008). Preparation of Fe(II)-montmorillonite by reduction of Fe(III)-montmorillonite with ascorbic acid. *Applied Clay Science*, *42*, 32–38.

Merola, R.B., Fournier, E.D., & McGuire, M.M. (2007). Spectroscopic investigations of Fe^{2+} complexation on nontronite clay. *Langmuir*, *23*, 1223–1226.

Milodowski, A.E., Cave, M.R., Kemp, S.J., Green, K., Williams, C.L., Shaw, R.A., Gowing, C.J.B., & Eatherington, N.D. (2007). Mineralogical Investigations of the Interaction Between Iron Corrosion Products and Bentonite from the NF-PRO Experiments (Phase *2*), 76 pp. British Geological Survey, Nottingham, UK.

Nose, S. (1984). A molecular-dynamics method for simulations in the canonical ensemble. *Molecular Physics*, *52*, 255–268.

O'Reilly, S.E., Watkins, J., & Furukawa, Y. (2005). Secondary mineral formation associated with respiration of nontronite, NAu-1 by iron reducing bacteria. *Geochemical Transactions*, *6*, 67.

Plimpton, S. (1995). Fast parallel algorithms for short-range molecular-dynamics. *Journal of Computational Physics*, *117*, 1–19.

Pouvreau, M., Greathouse, J.A., Cygan, R.T., & Kalinichev, A.G. (2017). Structure of hydrated gibbsite and brucite edge surfaces: DFT results and further development of the ClayFF classical force field with metal-O-H angle bending terms. *Journal of Physical Chemistry C*, *121*, 14757–14771.

Pouvreau, M., Greathouse, J.A., Cygan, R.T., & Kalinichev, A.G. (2019). Structure of hydrated kaolinite edge surfaces: DFT results and further development of the ClayFF classical force field with metal–O–H angle bending terms. *Journal of Physical Chemistry C*, *123*, 11628–11638.

Schaefer, M.V., Gorski, C.A., & Scherer, M.M. (2011). Spectroscopic evidence for interfacial Fe(II)−Fe(III) electron transfer in a clay mineral. *Environmental Science & Technology*, *45*, 540–545.

Smith, D.E., & Dang, L.X. (1994). Computer-simulations of NaCl association in polarizable water. *Journal of Chemical Physics*, *100*, 3757–3766.

Soltermann, D., Marques Fernandes, M., Baeyens, B., Dähn, R., Joshi, P.A., Scheinost, A.C., & Gorski, A.C. (2014a). Fe(II) uptake on natural montmorillonites. I. Macroscopic and spectroscopic characterization. *Environmental Science & Technology*, *48*, 8688–8697.

Soltermann, D., Marques Fernandes, M., Baeyens, B., Miehé-Brendlé, J., & Dähn, R. (2014b). Competitive Fe(II)–Zn(II) uptake on a synthetic montmorillonite. *Environmental Science & Technology*, *48*, 190–198.

Subramanian, N., Whittaker, M.L., Ophus, C., & Lammers, L.N. (2020). Structural implications of interfacial hydrogen bonding in hydrated Wyoming-montmorillonite clay. *Journal of Physical Chemistry C*, *124*, 8697–8705.

Teich-McGoldrick, S.L., Greathouse, J.A., Jové-Colón, C.F., & Cygan, R.T. (2015). Swelling properties of montmorillonite and beidellite clay minerals from molecular simulation: comparison of temperature, interlayer cation, and charge location effects. *Journal of Physical Chemistry C*, *119*, 20880–20891.

Teleman, O., Jonsson, B., & Engstrom, S. (1987). A molecular-dynamics simulation of a water model with intramolecular degrees of freedom. *Molecular Physics*, *60*, 193–203.

Van Groeningen, N., Thomas Arrigo, L.K., Byrne, J.M., Kappler, A., Christi, I., & Kretzschmar, R. (2020). Interactions of ferrous iron with clay mineral surfaces during sorption and subsequent oxidation. *Environmental Science: Processes & Impacts*, *22*, 1355–1367.

Whitley, H.D., & Smith, D.E. (2004). Free energy, energy, and entropy of swelling in Cs-, Na-, and Sr-montmorillonite clays. *Journal of Chemical Physics*, *120*, 5387–5395.

Zhou, H., Chen, M., Zhu, R., Lu, X., Zhu, J., & He, H. (2020). Coupling between clay swelling/collapse and cationic partition. *Geochimica et Cosmochimica Acta*, *285*, 78–99.

https://doi.org/10.1017/cmn.2026.10031 Published online by Cambridge University Press